

Predictions for measuring the cross power spectrum of the HI 21-cm signal and the Lyman- α forest using OWFA

Anjan Kumar Sarkar,^{a,1} Somnath Bharadwaj,^{a,b,2}
Tapomoy Guha Sarkar^{c,3}

^aCentre for Theoretical Studies, IIT Kharagpur, Kharagpur - 721302, India

^bDepartment of Physics, IIT Kharagpur, Kharagpur - 721302, India

^cBirla Institute of Technology and Science, Pilani - 333031, India

E-mail: anjan@cts.iitkgp.ernet.in, somnath@phy.iitkgp.ernet.in,
tapomoy@pilani.bits-pilani.ac.in

Abstract. We have studied the possibility of measuring the cross-correlation of the redshifted HI 21-cm signal and the Lyman- α forest using an upcoming radio-interferometric array OWFA and an spectroscopic observation like SDSS-IV. Our results shows that it is possible to have a 6σ detection of the cross-correlation signal with OWFA PII using an observing time of 200 hrs each in $N_p = 25$ independent fields-of-view. However, not much can be done beyond this using the cross-correlation signal for $z_c = 3.35$ and $B = 30$ MHz. Apart from this, we have also envisaged a situation where observations are carried out at $z_c = 3.05$ and 2.55 which lie closer to the peak of the quasar distribution at $z = 2.25$ and with a larger bandwidth of $B = 60$ MHz. We see that the SNR of the cross-correlation detection can be significantly enhanced to ~ 17 for $z_c = 2.55$ and $B = 60$ MHz. It is then possible to measure β_T and β_F individually with an $\text{SNR} \geq 5$ by combining the cross-correlation with the HI 21-cm auto-correlation measurements. We further find that a measurement of the binned cross-correlation power spectrum with $\text{SNR} \geq 5$ is also possible in several bins at $k \leq 0.3 \text{ Mpc}^{-1}$.

¹Corresponding author.

Contents

1	Introduction	1
2	Cross correlation signal of HI 21-cm and Lyman-α forest	4
3	Estimates for OWFA	6
4	Observational Considerations	10
5	Results	12
6	Summary and Conclusions	15
7	Acknowledgment	16

1 Introduction

Observation of the redshifted 21-cm signal from Neutral Hydrogen (HI) is considered to be a promising tool to map out the large scale structure of the universe from the post-reionization era ($z \leq 6$). Here, majority of the HI is hosted by the discrete sources which have the column number density, $N_{\text{HI}} \geq 2 \times 10^{20}$ atoms/cm² [1, 2]. Emission from these sources appears as the diffuse background in low frequency radio observations below 1420 MHz. Fluctuations in the background radiation in angular and the frequency scales, which are quantified through the HI power spectrum, carries the signature of the underlying source clustering at that epoch and can thereby be used to probe the large scale structure of the universe at high z [3–5]. Measurement of the HI power spectrum holds the potential of measuring the Baryon Acoustic Oscillations (BAO), which can be used to constrain the models of the dark energy [6–9]. The measurement of the HI power spectrum can be used further to constrain the background cosmological model [10, 11] and the neutrino mass [5, 12, 13]. In addition to the HI power spectrum, these fluctuations can also be used to probe the non-Gaussianities in the HI 21-cm signal, such as bispectrum [14, 15].

The Lyman- α forest are identified as the series of multiple Lyman- α absorption lines seen in the spectra of the background quasars. These absorption features arise from the tiny fluctuations in the HI density of the predominantly ionized diffuse IGM. Observations of the Lyman- α forest trace out the HI distribution in the direction of the line-of-sight of the observed quasars. On suitably large scales, the fluctuations in the HI 21-cm signal and transmitted flux of the quasars through the Lyman- α forest are expected to be a biased tracer of the matter distribution on large scales. Alike the HI 21-cm signal, the observations of the Lyman- α forest also finds use in a host of areas, such as the measurement of the matter power spectrum [16–18] and bispectrum [19–21], cosmological parameters [22, 23], constraints on neutrino mass

[24, 25], dark energy [26] and reionization history [27]. In addition to these, the recent Baryon Acoustic Oscillations Survey (BOSS) targets to probe the dark energy and the cosmic acceleration by measuring the large scale structure and imprints of BAO in the Lyman- α forest [28, 29].

The cross correlation of the HI 21-cm signal and the Lyman- α forest has been proposed to be a potential probe of the post-reionization era [30]. The cross correlation signal of the redshifted HI 21-cm emission and the Lyman- α forest carries a few unique features that makes it worthwhile to consider it a viable probe of the HI power spectrum apart from the auto-correlation of the individual signals. We begin with a brief discussion on a few aspects of the autocorrelation of the Lyman- α forest and the HI 21-cm signal to emphasize the features particular to the cross correlation signal. In the case of Lyman- α forest observations, the spectra can only be detected at discrete line of sights to the quasars. The Poisson noise due to the discrete sampling of the quasars, limits the accuracy with which one would be able to estimate the three dimensional auto power spectrum from a given survey. This limit is fixed by the quasar number density and the Signal-to-noise ratio for the each of the individual quasar spectrum. Both of these factors are specific to the instrument and observational strategy and one can not improve these for a given survey.

Contrary to the Lyman- α observations, redshifted HI 21-cm observations are sensitive to the HI distribution within the total field-of-view under observation. The accuracy of the measurement of the three-dimensional HI power spectrum depends on the array configuration of the instrument and the system noise. One can, in principle, use larger observation time to improve the precision with which one can measure the HI power spectrum. The redshifted HI 21-cm signal, however, remains buried in foregrounds from other sources like, galactic synchrotron radiation, point sources etc. that are several orders of magnitude larger than the HI signal [31]. Separating the foregrounds from the HI signal poses a serious challenge towards measuring the HI power spectrum. This is in contrast to the cross correlation signal, where foregrounds for the redshifted HI 21-cm signal and the Lyman- α forest are not correlated with each other. The problem of the foregrounds are thereby much less severe in case of the cross correlation signal as compared to that for the auto-correlation of the redshifted HI 21-cm signal, which gives the cross correlation an advantage over the redshifted 21-cm autocorrelation. In the presence of astrophysical foregrounds, one can be certain about the cosmological nature of the HI signal only if it is detected in a cross-correlation. In case of Lyman- α autocorrelation, the precision with which it is possible to measure the power spectrum is limited by the finite sampling of the QSOs. The issue of finite sampling of the QSOs is expected to be less sensitive for the cross correlation signal in comparison with the Lyman- α forest autocorrelation. Combined with the Lyman- α forest survey, a HI 21-cm observations can be suitably designed to measure the power spectrum with high accuracy using the cross correlation signal. The less severe issue of foregrounds subtraction compared to the redshifted HI 21-cm observations and prospects for higher SNR than the Lyman- α forest auto-correlation, serves the primary motivation towards using the cross correlation of the HI 21-cm signal and the Lyman- α forest.

There are a number of studies in the recent few years on using the cross-correlation of the HI 21-cm signal and the Lyman- α forest as the viable probe of the cosmology from the post reionization era [30]. The cross-correlation of the HI 21-cm signal and the Lyman- α forest can be used to measure the matter power spectrum in the post-reionization era [32, 33]. [34] have explored the possibility of using the cross correlation signal to make analytical estimates of the accuracy with which one would be able to detect the Baryon Acoustic Oscillations (BAO). In a subsequent study, [35] have looked for the possibility of detecting the three-dimensional cross correlation of the redshifted HI 21-cm signal and the Lyman- α forest using a future telescope like SKA-mid and a future experiment like Baryon Acoustic Oscillation Survey (BOSS). [36] have investigated the cross correlation signal in the non-linear regime using a complete state-of-the-art hydrodynamic N-body simulations and have found that the linear theory predictions for the shape and the amplitude of the cross correlation power spectrum even holds to a rather non-linear scales.

We have used OWFA to study the prospects of detecting the cross-correlation of the redshifted HI 21-cm signal and the Lyman- α forest from the spectroscopic observations like Baryon Oscillations Spectroscopic Survey or BOSS. OWFA is an upgradation of the Ooty Radio Telescope (ORT), which is expected to operate as a linear radio-interferometric array with a frequency of $\nu_0 = 326.5$ MHz, that corresponds to measuring the HI radiation from the redshift of $z_0 = 3.35$ [37, 38]. The ORT is 530 m long and 30 m wide parabolic cylindrical reflector, that is placed along the north-south direction on a hill of slope 11° which is same as the latitude of the place [39, 40]. It is thereby possible to observe a fixed part of the sky with a single rotation of the telescope. The feed system of the ORT consists of 1056 dipoles, which are placed end-to-end at 0.48 m apart from each other along the length of the cylinder. OWFA is capable to operate in two simultaneous independent interferometric modes - PI and PII [41]. The PI and PII have a total of 40 antennas and 264 antennas, where signals from 24 dipoles and 4 dipoles have been combined to form an single antenna element respectively. The operating bandwidth for the PII is 39 MHz.

A number of studies has been carried out in recent few years to explore the prospects of the OWFA. [41], have studied for the first time, the prospects for detecting the HI 21-cm signal using OWFA. Their study also contain detailed foreground predictions for OWFA. In a later study, [42] have used the Fisher matrix analysis to make estimates of the accuracy with which it would be possible to measure the amplitude of the HI power spectrum. In a recent study, [43] have made predictions based on Fisher matrix analysis for constraining the shape of the HI power spectrum over the k -range probed by the OWFA phase II.

We have used the Fisher matrix analysis to make an estimate of the accuracy with which it would be possible to measure the cross correlation power spectrum using the 21-cm observations with OWFA and the spectroscopic observation like BOSS of SDSS-IV. We have carried out our analysis to study prospects of measuring the cross correlation power spectrum from two different aspects. On the first hand, We have computed the expected signal-to-Noise ratios (SNR) for measuring the amplitude of the cross correlation power spectrum, A_{FT} . We assumed that both the HI distribution

traces the underlying matter power spectrum on large scales and the shape of the matter power spectrum is specified precisely by the standard Λ CDM cosmological model. In addition to this, we have also made estimates for detecting β_T , redshift space distortion parameter for the HI power spectrum and β_F , the redshift space distortion parameter for the Lyman- α forest. This is the first full covariance matrix analysis of the 21-cm and Ly - α crosscorrelation using the observationally meaningful visibility based approach.

Further, we have explored the possibility of directly measuring the binned cross correlation power spectrum without any prior information about its amplitude and shape. Several astrophysical processes can alter the shape of the cross correlation power spectrum without any reference to the change in the matter power spectrum. Further, changes in the background cosmological model will be reflected as the changes in the shape of the matter power spectrum via several effects like redshift space distortion, Alcock-Paczynski (AP) effect etc. For this purpose, we have divided the entire k -range into a number of k -bins and have used the Fisher matrix analysis to estimate the SNR for measuring the amplitude in each of these k -bins. We have used the transfer function of the baryonic matter power spectrum of [44] with cosmological parameters taken from [45]. Constraining the shape of the cross-correlation power spectrum directly gives us a novel way to measure various parameters of astrophysical and cosmological interest.

The present paper is outlined as follows. In section 2, we present a discussion about the cross correlation power spectrum between of the HI 21-cm signal and Lyman- α forest. In section 3, we give a brief overview of the parameters of the OWFA and have calculate the Fisher matrix of the cross-correlation of the visibilities of the HI 21-cm signal and the Lyman- α forest for OWFA. In section 4, we discuss the results of the Fisher matrix analysis for obtaining constraints on the parameters A_{FT} , β_T and β_F . We have also presented estimates for measuring the binned power spectrum in this section. The concluding Section 5 summarizes the results of our analysis.

2 Cross correlation signal of HI 21-cm and Lyman- α forest

The brightness temperature fluctuations $\delta_T(\hat{n}, z)$ and the dimensionless fluctuations $\delta_F(\hat{n}, z)$ of transmitted flux are the quantities of interest for the redshift HI 21-cm signal and the Lyman α forest respectively. Here we consider observation in a region of angular extent $L \times L$ and redshift band B which respectively correspond to the field of view (FoV) and the frequency band of the radio telescope used for the 21-cm observations. In the flat-sky approximation, we can express the unit vector \hat{n} as $\hat{n} = \hat{m} + \vec{\theta}$ where $\vec{\theta}$ is a two-dimensional vector on the plane of the sky and \hat{m} is a unit vector along the line-of-sight to the centre of the FoV. We further assume that the band B is divided into N_c number of channels each of width Δz_c (which corresponds to the frequency channel width of the radio telescope), and we can express $z = z_c + \Delta z_n$ where z_c is the redshift at the center of the band, $\Delta z_n = n\Delta z_c$ and $-N_c/2 < n \leq +N_c/2$.

It is convenient to decompose the fluctuations $\delta_\alpha(\vec{\theta}, \Delta z_n)$ (here $\alpha = F, T$) into

Fourier modes using [34]

$$\delta_\alpha(\vec{\theta}, \Delta z_n) = (BL^2)^{-1} \sum_\tau \sum_{\vec{U}} \Delta_\alpha(\vec{U}, \tau) e^{2\pi i(\vec{U} \cdot \vec{\theta} + \tau \Delta z_n)} \quad (2.1)$$

where \vec{U} and τ are the Fourier conjugates of $\vec{\theta}$ and Δz_n respectively.

We quantify the statistical properties of these fluctuations using the power spectra $\mathcal{P}_{\alpha\gamma}(\vec{U}, \tau_n)$ which, in the limit of $L \rightarrow \infty$, are defined through

$$\langle \Delta_\alpha(\vec{U}, \tau_m) \Delta_\gamma^*(\vec{U}', \tau_n) \rangle = B \delta_{m,n} \delta^2(\vec{U} - \vec{U}') \mathcal{P}_{\alpha\gamma}(U, \tau_n) \quad (2.2)$$

where $\delta_{m,n}$ is the Kronecker delta and $\delta^2(\vec{U} - \vec{U}')$ is the Dirac delta function. Here the power spectrum $\mathcal{P}_{TT}(U, \tau_m)$ and $\mathcal{P}_{FF}(U, \tau_m)$ respectively refer to the 21-cm and the Lyman- α forest auto-correlation signals whereas $\mathcal{P}_{TF}(U, \tau_m)$ refers to cross-correlation between these two signals. Note that we have discrete values $\tau_m = m/B$ with $-N_c/2 < m \leq N_c/2$.

On sufficiently large length-scales it is reasonable to assume that the 21-cm and the Lyman- α forest signals are both linearly related to the underlying matter fluctuations whereby we can express the power spectra $\mathcal{P}_{\alpha\gamma}(U, \tau_m)$ as

$$\mathcal{P}_{\alpha\gamma}(U, \tau_m) = F_{\alpha\gamma}(\mu) P(k) \quad (2.3)$$

where $P(k)$ is the dark matter power spectrum and the comoving wave vector \vec{k} with $k = |\vec{k}|$ has components $k_\perp = 2\pi\vec{U}/r$ and $k_\parallel = 2\pi H(z)\tau_m/c$ respectively perpendicular and parallel to the line of sight. Here r and $H(z)$ respectively refer to the co-moving distance and the Hubble parameter corresponding to z_c and

$$F_{\alpha\gamma}(\mu) = H(z)(cr^2)^{-1} C_\alpha C_\gamma (1 + \beta_\alpha \mu^2) (1 + \beta_\gamma \mu^2) \quad (2.4)$$

Where $\mu = k_\parallel/k$. For the Lyman- α forest we have used the values $C_F = (-0.13, -0.29, -0.29)$ and $\beta_F = (1.58, 1.13, 1.13)$ at redshifts $z_c = (2.55, 3.05, 3.35)$ respectively, this is based on the fit to the 1D Lyman- α power spectrum presented in [46]. For the HI 21-cm signal we have used $C_T = (\bar{T} x_{HI} b_{HI})$ and $\beta_T = f(\Omega)/b_{HI}$ where $\bar{T}(z)$ is the characteristic 21-cm brightness temperature [47], $f(\Omega)$ is the growth rate of linear perturbations, x_{HI} is the mean neutral hydrogen fraction and b_{HI} is the HI bias. Note that $A_c = C_F C_T$ is the amplitude of the cross-correlation power spectrum, whereas $A_F = C_F^2$ and $A_T = C_T^2$ refer to amplitudes of the respective auto-correlation power spectra.

DLA observations [2, 48, 49] in the redshift range of our interest give a measurement of $\Omega_{HI} \approx 10^{-3}$ which corresponds to $x_{HI} = 0.02$. Semi-numerical simulations [50–52] of the expected 21-cm signal have been found to be consistent with a linear, scale-independent HI bias at scales $k \leq 1 \text{ Mpc}^{-1}$. We have used a recent fit to the simulated $b_{HI}(z)$ [53] for the present analysis. The value of $f(\Omega)$ was calculated using the Λ CDM cosmological parameters [45].

So far we have considered the fluctuations in the transmitted flux of Lyman- α forest $\delta_F(\vec{\theta}, \Delta z_n)$ to be a continuous field that is defined at each $\vec{\theta}$ in the FoV. In

reality, this is only observed along a few, discrete lines of sight to background quasars. We incorporate this through a sampling function

$$\rho(\vec{\theta}, \Delta z_n) = \frac{\sum_a \delta^2(\vec{\theta} - \vec{\theta}_a)}{\bar{n}_Q} \quad (2.5)$$

where the sum runs over the background quasars in the FoV, and \bar{n}_Q is the angular number density of background quasars. Accounting for the discrete sampling and also the pixel noise in the observation, the observed dimensionless fluctuation of the Lyman- α forest transmitted flux can be expressed as

$$\delta_{Fo}(\vec{\theta}, \Delta z_n) = \rho(\vec{\theta}, \Delta z_n) [\delta_F(\vec{\theta}, \Delta z_n) + \delta_{FN}(\vec{\theta}, \Delta z_n)] \quad (2.6)$$

where $\delta_{FN}(\vec{\theta}, \Delta z_n)$ is the contribution from the pixel noise.

We model the pixel noise $\delta_{FN}(\vec{\theta}, \Delta z_n)$ as a Gaussian random variable with the assumption that the noise in different pixels ($\vec{\theta}_a, \Delta z_n$) are uncorrelated, ie.

$$\langle \delta_{FN}(\vec{\theta}_a, \Delta z_m) \delta_{FN}^*(\vec{\theta}_b, \Delta z_n) \rangle = \sigma_{FN}^2 \delta_{ab} \delta_{mn} \quad (2.7)$$

where σ_{FN}^2 is the variance of the pixel noise. We can now write the observed Lyman- α forest power spectrum, $\mathcal{P}_{FFo}(\vec{U}, \tau_m)$ as [34]

$$\mathcal{P}_{FFo}(\vec{U}, \tau_m) = \mathcal{P}_{FF}(\vec{U}, \tau_m) + (\bar{n}_Q)^{-1} [p_{1D}(\tau_m) + \sigma_{FN}^2 \Delta z_c] \quad (2.8)$$

where $p_{1D}(\tau_m)$ is the Lyman- α forest 1D power spectrum measured in various observations. [46, 54]. We note that the term $(\bar{n}_Q)^{-1} [\dots]$ in eq. (2.8) arises due the finite quasar sampling, and this term tends to zero in the continuum limit ($\bar{n}_Q \rightarrow \infty$).

3 Estimates for OWFA

OWFA PII is a N-S linear array of $N_A = 264$ antennas each of which has a rectangular aperture of dimension $b \times d$, where $b = 30$ m is the width of the ORT parabolic cylinder and $d = 1.92$ m along the length of the cylinder. The antennas are arranged end to end along the length of the cylinder resulting in an antenna separation of $d = 1.92$ m between the centers of two successive antennas. Using a coordinate system with the x and y axes along the length and width of the array respectively, the aperture power pattern can be written as, [41]

$$\tilde{a}(\vec{U}, \nu) = \left(\frac{\lambda^2}{bd} \right) \Lambda \left(\frac{U_x \lambda}{d} \right) \Lambda \left(\frac{U_y \lambda}{b} \right). \quad (3.1)$$

where $\Lambda(x)$ is the triangular function defined as, $\Lambda(x) = 1$ for $|x| < 1$ and zero elsewhere. Here $\tilde{a}(\vec{U}, \nu)$ is the Fourier transform of the OWFA PII primary beam pattern, $A(\vec{\theta}, \nu) = \text{sinc}^2(\pi d \theta_x / \lambda) \text{sinc}^2(\pi b \theta_y / \lambda)$ with corresponds to a FoV of $(\lambda/d, \lambda/b) = (27^\circ, 1.75^\circ)$.

The one-dimensional configuration of the antennas allows us to write the baselines \vec{U}_n as

$$\vec{U}_n = n \left(\frac{d}{\lambda} \right) \hat{i} \quad (1 \leq n \leq N_A - 1). \quad (3.2)$$

The OWFA baselines are highly redundant, and any given baseline \vec{U}_n has a redundancy factor of $(N_A - n)$. The visibility $\mathcal{V}_T(\vec{U}_a, \nu_n)$ measured at any baseline \vec{U}_n and frequency channel ν_n is related to $\delta I(\vec{\theta}, \nu_n)$ the specific intensity fluctuations on the sky as

$$\mathcal{V}_T(\vec{U}_a, \nu_n) = \int A(\vec{\theta}, \nu_n) \delta I(\vec{\theta}, \nu_n) e^{2\pi i \vec{U}_a \cdot \vec{\theta}} d^2\theta + \mathcal{N}(\vec{U}_a, \nu_n), \quad (3.3)$$

where $\mathcal{N}(\vec{U}_a, \nu_n)$, is the additive noise which is inherent to radio-interferometric observations. We further assume that the noise in different baselines and frequency channels is uncorrelated, and the real and imaginary components of $\mathcal{N}(\vec{U}_a, \nu_n)$ both have zero mean and standard deviation

$$\sigma_T = \frac{\sqrt{2} k_B T_{sys}}{\eta A \sqrt{\Delta \nu_c t}} \quad (3.4)$$

where T_{sys} is the system temperature, η is the aperture efficiency, $A = b \times d$ is the aperture area, $\Delta \nu_c$ is the frequency channel width which also corresponds to Δz_c and t is the observation time. Note that we have assumed a single polarization (which is the case for OWFA) and not incorporated the baseline redundancy in eq. (3.4).

For the redshifted 21-cm signal we replace ν_n with Δz_n using the conversion $\nu = 1420/(1+z)$, and use $\delta I(\vec{\theta}, \nu) = Q_\nu \delta_T(\vec{\theta}, \nu)$ where $Q_\nu = 2k_B/\lambda^2$ is the conversion factor from brightness temperature to specific intensity in the Rayleigh-Jeans approximation. The baselines \vec{U} , the primary beam pattern $A(\vec{\theta}, \nu)$ and Q_ν all change with frequency. For the present analysis we assume that this variation is relatively small ($\sim 15 - 20\%$ as shown for OWFA PI in [55]) across the observing bandwidth and we hold these quantities fixed at the values corresponding to central frequency ν_c .

It is convenient to decompose the visibilities $\mathcal{V}_T(\vec{U}, \Delta z_n)$ into delay channels [56], using

$$v_T(\vec{U}, \tau_m) = \Delta z_c \sum_n e^{2\pi i \tau_m (n \Delta z_c)} \mathcal{V}_T(\vec{U}, \Delta z_n) \quad (3.5)$$

whereby we can express $v_T(\vec{U}, \tau_m)$ in terms of $\Delta_T(\vec{U}', \tau_m)$ (eq. 2.1) as

$$v_T(\vec{U}_a, \tau_m) = Q \int \tilde{a}(\vec{U}_a - \vec{U}') \Delta_T(\vec{U}', \tau_m) d^2U' + n(\vec{U}', \tau_m). \quad (3.6)$$

and the noise contribution now has the property

$$\langle n^*(\vec{U}_a, \tau_n) n(\vec{U}_b, \tau_m) \rangle = 2B \Delta z_c \sigma_T^2 \delta_{a,b} \delta_{n,m}. \quad (3.7)$$

A Lyman- α forest survey typically covers a large area of the sky (e.g. BOSS covers an area of 6373.2 deg² for DR10 of SDSS [57]) as compared to the OWFA FoV. Considering OWFA observations in a particular pointing direction, the 32-cm visibility signal will be maximally correlated with the Lyman- α forest signal when

they both originate from exactly the same region, and the correlation will fall off (~ 0) if the regions from where the two signals originate have no overlap. An uncorrelated component in the Lyman- α forest will contribute to the variance without contributing to the cross-correlation signal, thereby degrading the signal to noise ratio. For the cross-correlation signal it is most advantageous to exactly match the spatial regions which are probed by the 21-cm and the Lyman- α respectively. We address this by multiplying the Lyman- α forest data $\delta_{Fo}(\vec{\theta}, \Delta z_n)$ with the OWFA primary beam pattern $A(\vec{\theta}, \nu_c)$ and restricting the redshift band B to exactly match the OWFA coverage. In analogy with the 21-cm signal visibilities, we also decompose the Lyman- α forest signal into visibilities (eq. 3.3) at the OWFA baselines. It is useful to express these Lyman- α visibilities as

$$v_F(\vec{U}, \tau_n) = \int \tilde{a}(\vec{U} - \vec{U}') \Delta_{Fo}(\vec{U}', \tau_n) d^2U'. \quad (3.8)$$

Note that $\Delta_{Fo}(\vec{U}', \tau_n)$ includes the pixel noise (eq. 2.6) and there is no other additive noise term in eq. (3.8).

We use the visibility correlation

$$C_{ab}(m) = \langle v_T^*(\vec{U}_a, \tau_m) v_F(\vec{U}_b, \tau_m) \rangle \quad (3.9)$$

to quantify the cross-correlation signal predictions for OWFA, and using equations (2.2), (3.6) and (3.8) we obtain

$$C_{ab}(m) = Q B \int \tilde{a}(\vec{U}_a - \vec{U}') \tilde{a}(\vec{U}_b - \vec{U}') P_{FT}(\vec{U}', \tau_m) d^2U'. \quad (3.10)$$

We note that the signal at different τ_m values are uncorrelated (eq. 2.2), and it is not necessary to consider such correlations. The visibilities measured at OWFA are correlated only for the same baseline ($a = b$) and adjacent baselines ($a = b \pm 1$). Further the correlation for adjacent baselines is roughly one fourth the correlation at the same baseline [41], and all other possible correlations are zero. It is convenient to introduce a more compact notation using $\mathbf{P}_a(m)$ with $1 \leq a \leq 2N_A - 3$ to denote the non-zero elements of the visibility correlation $C_{ab}(m)$. The first $N_A - 1$ elements of $\mathbf{P}_a(m)$ denote the correlations at the same baseline ($\mathbf{P}_a(m) = C_{ab}(m)$ with $b = a$), and the subsequent $N_A - 2$ elements of $\mathbf{P}_a(m)$ denote the correlations at the adjacent baselines ($\mathbf{P}_a(m) = C_{ab}(m)$ with $b = a + 1$). The error covariance for \mathbf{P}_a can be calculated using

$$\langle \Delta \mathbf{P}_{a_1}(m) \Delta \mathbf{P}_{a_2}(m) \rangle = \frac{1}{2} [C_{a_1 a_2}(m) C_{b_1 b_2}(m) + C_{a_1 b_2}(m) C_{a_2 b_1}(m)] + \quad (3.11)$$

$$\frac{1}{8} [F_{a_1 a_2}(m) T_{b_1 b_2}(m) + F_{b_1 b_2}(m) T_{a_1 a_2}(m) + F_{a_1 b_2}(m) T_{a_2 b_1}(m) + F_{a_2 b_1}(m) T_{a_1 b_2}(m)]. \quad (3.12)$$

where b_1 and b_2 are indices associated with a_1 and a_2 respectively. We find that the error covariance in the above equation (eq. 3.12) depends on terms of two different types, the first being the product of the cross correlations signals eg. $C_{a_1 b_2}(m) C_{a_2 b_1}(m)$ and

the second being the product of the auto correlation of the Lyman- α forest and the HI 21-cm signal, eg. $F_{b_1 b_2}(m) T_{a_1 a_2}(m)$. We calculate the auto correlation signals of the HI 21-cm signal and the Lyman- α forest respectively using

$$T_{ab}(m) = BQ^2 \int \tilde{a}(\vec{U}_a - \vec{U}') \tilde{a}(\vec{U}_b - \vec{U}') P_{TT}(\vec{U}', \tau_m) d^2 U' + 2B \sigma_T^2 \Delta z_c (N_A - a)^{-1} \delta_{a,b} \quad (3.13)$$

and

$$F_{ab}(m) = B \int \tilde{a}(\vec{U}_a - \vec{U}') \tilde{a}(\vec{U}_b - \vec{U}') P_{FFo}(\vec{U}', \tau_m) d^2 U' \quad (3.14)$$

where the term $(N_A - a)^{-1}$ in eq (3.13) arises from the OWFA baseline redundancy.

We have used the Fisher matrix

$$\mathbf{F}_{pq} = \sum_m \mathbf{P}_{a_1, p}(m) [\langle \Delta \mathbf{P}_{a_1}(m) \Delta \mathbf{P}_{a_2}(m) \rangle]^{-1} \mathbf{P}_{a_2, q}(m), \quad (3.15)$$

to estimate the accuracy for parameter estimation using OWFA measurements of the 21-cm and Lyman- α cross-correlation signal, here the indices p and q refer to the different parameters whose values we wish to estimate from the observations. For most of our analysis we have considered three parameters $q_1 = \ln(A_c)$, $q_2 = \ln(\beta_T)$ and $q_3 = \ln(\beta_F)$ which correspond to the amplitude of the cross-correlation signal, the redshift space distortion parameter for the 21-cm signal and the redshift space distortion parameter for the Lyman- α forest respectively. The elements $\delta A_c/A_c = 1/\sqrt{\mathbf{F}_{11}}$, $\delta \beta_T/\beta_T = 1/\sqrt{\mathbf{F}_{22}}$ and $\delta \beta_F/\beta_F = 1/\sqrt{\mathbf{F}_{33}}$ provide estimates of the conditional fractional errors in the respective parameters. We have inverted the Fisher matrix to calculate the marginalized errors reported subsequently in this paper.

The dependence on the HI 21-cm observation time t enters into the Fisher matrix (eq. 3.15) through the error covariance (eq. 3.12). For small observation times, the noise (second term in eq. 3.13) dominates over the HI 21-cm signal and we have $T_{ab}(m) \propto 1/t$. Further, the terms of the form $T_{ab}(m)F_{ab}(m)$ dominate the error covariance $\langle \Delta \mathbf{P}_{a_1}(m) \Delta \mathbf{P}_{a_2}(m) \rangle$ whereby we expect the Fisher matrix to increase linearly with t , ie. $\mathbf{F}_{pq} \propto t$. For large observation times, the noise (second) term in eq. (3.13) is considerably below the HI 21-cm signal and we expect $T_{ab}(m)$ and also the Fisher matrix to saturate at a value which is independent of the observation time.

Apart from the observation time, the Fisher matrix (eq. 3.15) also depends on the quasar number density \bar{n}_Q and the pixel noise σ_{FN} through \mathcal{P}_{FFo} (eq. 2.8) which affects the error covariance (eq. 3.12) through $F_{ab}(m)$ (eq. 3.14). We see that it is possible to decrease the error covariance by increasing the quasar number density \bar{n}_Q . It is also possible to decrease the error covariance by reducing σ_{FN} . We expect the error covariance and the Fisher matrix to saturate in the continuum limit, $\bar{n}_Q \rightarrow \infty$. We finally note that the limits $\bar{n}_Q \rightarrow \infty$ and $t \rightarrow \infty$ corresponds to the cosmic variance which sets the lower and upper limits for the error covariance and the Fisher matrix respectively. For the present analysis consider $\bar{n}_Q(z)$ and σ_{FN} to be fixed as given by SDSS DR-14 [58], and discuss these in somewhat more detail in the subsequent section.

The analysis of this paper is mainly focused on the HI 21-cm and Lyman- α forest cross-correlation signal. As discussed earlier, we expect the Fisher matrix for the cross-correlation to scale as $\mathbf{F}_{pq} \propto t$ for small observation times and subsequently saturate for large observation times. For comparison we also consider the HI 21-cm auto-correlation signal. In contrast to the error covariance for the cross-correlation (eq. 3.12), the error covariance for the 21-cm auto-correlation only has terms of the form $\langle \Delta \mathbf{P}_{a_1}(m) \Delta \mathbf{P}_{a_2}(m) \rangle \sim \propto T_{a_1 b_2}(m) T_{P a_2 b_1}(m)$ (eq. 7 of [59]). We therefore expect the Fisher matrix for the auto-correlation to scale as $\mathbf{F}_{pq} \propto t^2$ for small observation times and subsequently saturate at the cosmic variance limit for large observation times. It is useful to note that the Fisher matrix for the auto-correlation signal increases more rapidly than that for the cross-correlation signal as the observation time is increased. It also follows that for small observation times we expect the errors in parameter estimation to scale as $\delta q \propto 1/\sqrt{t}$ and $\delta q \propto 1/t$ for the cross-correlation and auto-correlation signals respectively. In both cases the errors saturate at large t .

4 Observational Considerations

We have carried out our present analysis considering OWFA PII which operates at a central frequency $\nu_c = 326.5$ MHz that corresponds to HI at redshift $z_c = 3.35$. Although the actual bandwidth of the OWFA PII is 39 MHz, for the present analysis we have used a bandwidth of $B = 30$ MHz that gives access to observation in the range $3.15 \leq z \leq 3.55$. It is worthwhile and interesting to consider the possibility of modifying the antenna system to increase the OWFA bandwidth. In order to assess the improvement that would be achieved by increasing the bandwidth, we have also performed the entire analysis considering a larger bandwidth of $B = 60$ MHz.

We have used the quasar number distribution from the DR14 of SDSS [58] which gives the binned quasar numbers $\Delta N(z)$ over different redshifts in the range $0 \leq z \leq 4$, with a bin of width $\Delta z_{\text{bin}} = 0.04$. We see that the quasar distribution peaks at $z = 2.25$, with $\Delta N(z) \sim 30000$, and falls off as we move away from the peak. We further see that at $z \geq 3$, $\Delta N(z)$ goes below one-tenth of the value at $z = 2.25$. Note that SDSS DR14 has a total angular coverage of $14,555 \text{ deg}^2$ ¹.

The number of quasars available for estimating the cross correlation signal in the OWFA band centered at the redshift, $z_c = 3.35$ is quite low. We have explored the possibility to increase the number of quasars by considering observations at a redshift nearer to the peak of the quasar distribution. For the purpose of the present analysis, we have considered the possibility of modifying the OWFA system for observation at redshifts $z_c = 3.05$ and $z_c = 2.55$ that correspond to HI 21-cm observation at frequencies $\nu_c = 350$ MHz and $\nu_c = 400$ MHz respectively. The number of quasars increases by a factor of ~ 3 and ~ 5 respectively as compared to that at redshift $z_c = 3.35$.

Given a quasar at redshift z_Q , for the cross-correlation analysis we have excluded the region $10,000 \text{ km s}^{-1}$ blue-ward of the Lyman- α emission peak of the quasar because of the quasar proximity effect [60, 61]. We have further only considered the part of the

¹<http://www.sdss.org/dr14/scope/>

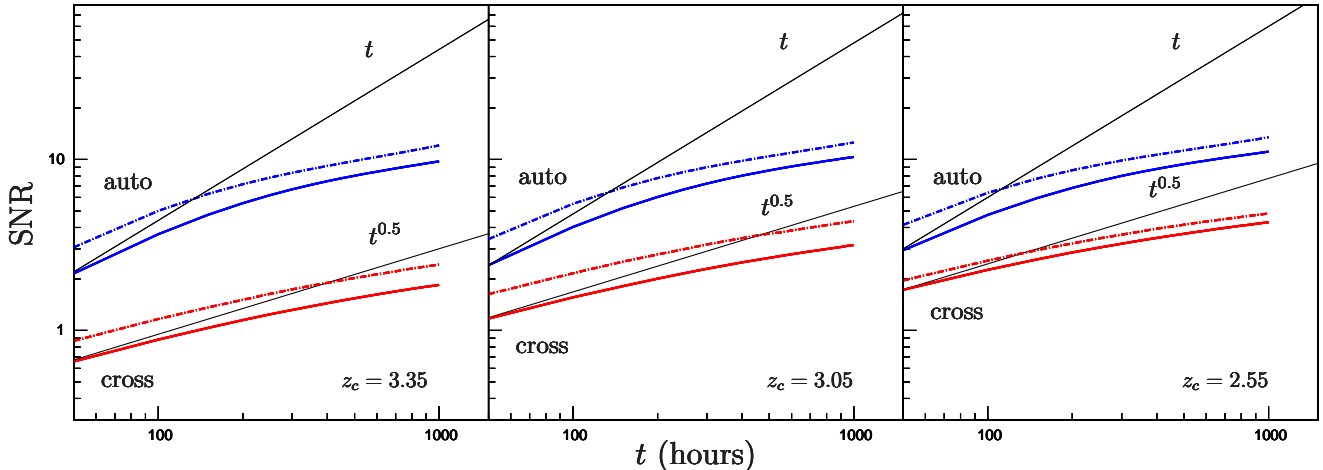


Figure 1. Shows the plot of the predicted SNR for measuring A_c (red lines) and C_T (black lines) versus the observing time t for the different redshifts and bandwidths considered for our analysis. The solid black lines in each figure shows the expected behaviour of the SNR for measuring A_c and C_T with t respectively, ie. $\text{SNR} \propto t^{0.5}$ and $\text{SNR} \propto t$, in the limit of small observing times.

spectrum beyond $1,000 \text{ km s}^{-1}$ red-ward of the Lyman- β line or the O-VI lines to avoid any possibility of confusing the Lyman- α forest with the Lyman- β or O-VI absorption lines in the quasar spectrum. For the given quasar, this restricts the redshift range across which the quasar spectrum can be used for the cross-correlation analysis. The overlap between this redshift range and the OWFA 21-cm band can vary depending on the values of z_Q , z_c and B . We have accounted for both complete and partial overlap in estimating the mean quasar number density $\bar{n}_Q(z_c)$ available for the cross-correlation analysis. The actual signal to noise ratio (SNR) varies from quasar to quasar, and this can be as large as $\text{SNR}=10$ for the bright quasars. To keep the analysis simple we have assumed an uniform value $\text{SNR} = 5$ which implies $\sigma_{FN} = 0.2$ in eq. (2.8).

The discussion till now is restricted to 21-cm observations in a single pointing direction. As mentioned earlier, the OWFA FoV is much smaller than the area covered by Lyman- α surveys like BOSS, and it is worthwhile to also consider the possibility of extending the analysis to a situation where 21-cm observations are carried out in N_p different pointing directions. In the present work we have assumed that we obtain independent cross-correlation signals from each different pointing direction whereby the Fisher matrix for the combined observation is N_p times the Fisher matrix for a single pointing direction. The results from our Fisher matrix analysis are presented in the section to follow.

5 Results

We begin our analysis by considering the prospects of measuring the amplitude of the cross correlation signal A_c using OWFA PII. Figure 1 shows how the predicted signal-to-noise ratio (SNR) for measuring A_c varies with the observing time t . We have calculated the SNR for measuring A_c using $\text{SNR} = 1/\sqrt{[F^{-1}]_{11}}$ which is marginalized over β_T and β_F the two other parameters in our analysis. We first consider the left panel of the Figure 1 which shows the results at $z = 3.35$ where OWFA is expected to operate at present. As discussed in Section 3, at small observation times we expect the SNR to increase as, $\text{SNR} \propto t^{0.5}$. We see that for t in the range 50 – 100 hrs the SNR grows as $\text{SNR} \propto t^{0.43}$ which is somewhat slower compared to $\text{SNR} \propto t^{0.5}$. We may expect the $\text{SNR} \propto t^{0.5}$ regime to be restricted to observing times $t < 50$ hrs. We see that for $B = 30$ MHz the SNR increases to ~ 1 for $t \sim 200$ hrs. The SNR increases very slowly beyond this, and it only increases by a factor of ~ 1.5 for $t \sim 1000$ hrs. Considering a larger bandwidth of $B = 60$ MHz, we see that the SNR increases by a factor of ~ 1.3 as compared to $B = 30$ MHz.

As mentioned earlier, the number of quasars available for the cross-correlation analysis peaks around $z \sim 2.25$. In order to see if it is possible to improve the prospects of a measurement by moving closer to the peak, we have considered observations centered at two other redshifts namely $z_c = 3.05$ and 2.55 for which the results are shown in the middle and right panels respectively. Considering $B = 30$ MHz we see that it is possible to achieve $\text{SNR} \sim 2$ and ~ 3 with $t \sim 200$ hrs observations at $z_c = 3.05$ and 2.55 respectively. Considering $B = 60$ MHz, the SNR values increase by factors of 1.4 and 1.1 at $z_c = 3.05$ and 2.55 respectively. In all cases, the SNR increases very slowly for observation times $t > 200$ hrs, and it is not very meaningful to consider deeper observation in a single FoV. Based on this, we consider a situation where $N_p = 25$ independent fields-of-view are observed for 200 hrs each. The predicted SNR values for measuring A_c are summarized in the Table 1. We see that a $5 - \sigma$ detection is possible in all the cases considered here. We have $\text{SNR} \sim 6$ at $z_c = 3.35$ with $B = 30$ MHz. The SNR increases to ~ 15 at $z_c = 2.55$ which is closer to the peak of the quasar distribution, the SNR also increases by a factor of 1.1 to 1.5 if the bandwidth is doubled.

For comparison, we have also shown the SNR for measuring the HI 21-cm auto-correlation signal C_T (blue lines). We see that in this case the SNR varies rather rapidly with t and subsequently saturates at a larger t as compared to the SNR for measuring A_c . For $B = 30$ MHz, it is possible to have a measurement with $\text{SNR} \sim 5$ for $t \sim 150$ hrs at $z_c = 3.35$. We further see that the SNR increases by a factor of ~ 1.1 and ~ 1.2 at $z_c = 3.05$ and 2.55 respectively. The SNR increases by a factor of 1.4 for all the redshifts considered here if the bandwidth is doubled.

We have next considered the prospects of the joint measurement of the parameters β_T and β_F marginalizing over A_c . We have considered an observing time of 200 hrs each in $N_p = 25$ independent fields-of-view. We find that the relative errors in β_T and β_F are large and are highly anti-correlated. We have identified the combinations $q_1 = (\beta_F^{0.83} \beta_T^{0.55})$ and $q_2 = (\beta_F^{-0.55} \beta_T^{0.83})$ for which the errors are uncorrelated at $z_c = 3.35$.

Table 1. Predicted SNR for measuring A_c with an observation time of 200 hrs each in 25 independent fields-of-view for the different redshifts and bandwidths considered here.

z	3.35	3.35	3.05	3.05	2.55	2.55
B (MHz)	30	60	30	60	30	60
SNR	~ 6	~ 9	~ 10	~ 14	~ 15	~ 17

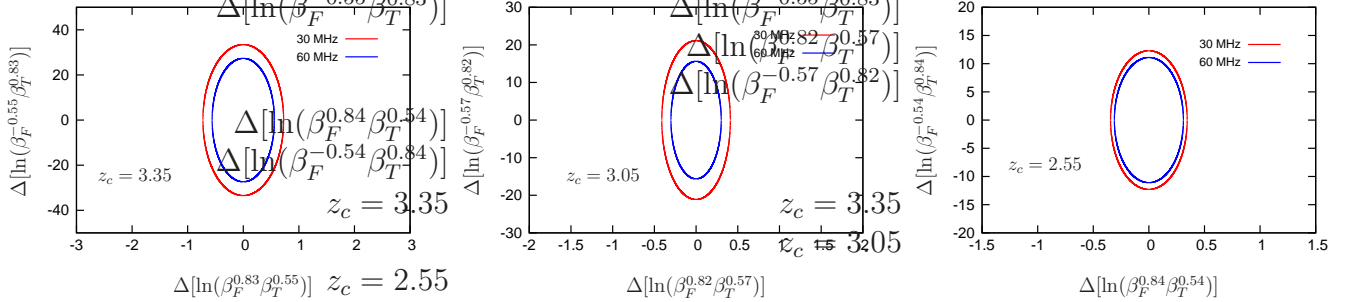


Figure 2. Shows the errors on the joint measurement of the parameters $q^{ab} = \ln(\beta_F^a \beta_T^b)$, with an observing time of 200 hrs each in $N_p = 25$ independent fields-of-view for the different redshifts and bandwidths considered in our analysis.

Note that the values of the exponents change slightly with z_c . For $z_c = 3.35$ (left panel of Figure 2) with $B = 30$ MHz we have relative errors of ~ 1 and ~ 40 for q_1 and q_2 respectively. The errors on q_1 and q_2 respectively decrease by factors of 2 and 1.3 for $B = 60$ MHz. Considering $z_c = 3.05$ (central panel) for $B = 30$ MHz we have relative errors of ~ 0.5 and ~ 20 for q_1 and q_2 respectively, and these decrease respectively by factors of 1.6 and 1.3 for $B = 60$ MHz. Considering $z_c = 2.55$ (right panel) for $B = 30$ MHz we have relative errors of ~ 0.4 and ~ 15 for q_1 and q_2 respectively, and these decrease respectively by factors of 1.3 and 1.25 for $B = 60$ MHz.

In the previous discussion we find that the prospects of a joint measurement of the combinations of β_F and β_T are quite low, and at best possible a 3σ measurement is possible at $z_c = 2.55$ for $B = 60$ MHz. However, it is worthwhile to note that it is possible to measure β_T at a comparatively higher SNR using HI 21-cm observation alone. As can be seen from Figure 1 (blue lines), the SNR for the auto correlation signal increases more rapidly with t as compared to the cross-correlation. For the auto-correlation it is more advantageous to consider deeper observations of $t \sim 1000$ hrs, and for the present analysis we consider a situation where such observations are carried out in $N_p = 5$ independent fields of view to measure the value of β_T from the auto-correlation signal. We find that it is possible to measure β_T with errors $\Delta\beta_T/\beta_T \sim 0.24, 0.22, 0.18$ respectively at $z_c = 3.35, 3.05, 2.55$ for $B = 30$ MHz. The errors decrease by a factor of 2.3 for $B = 60$ MHz. We consider the relative error $\Delta\beta_F/\beta_F$ in measuring β_F given that the measurement of β_T comes from the HI 21-

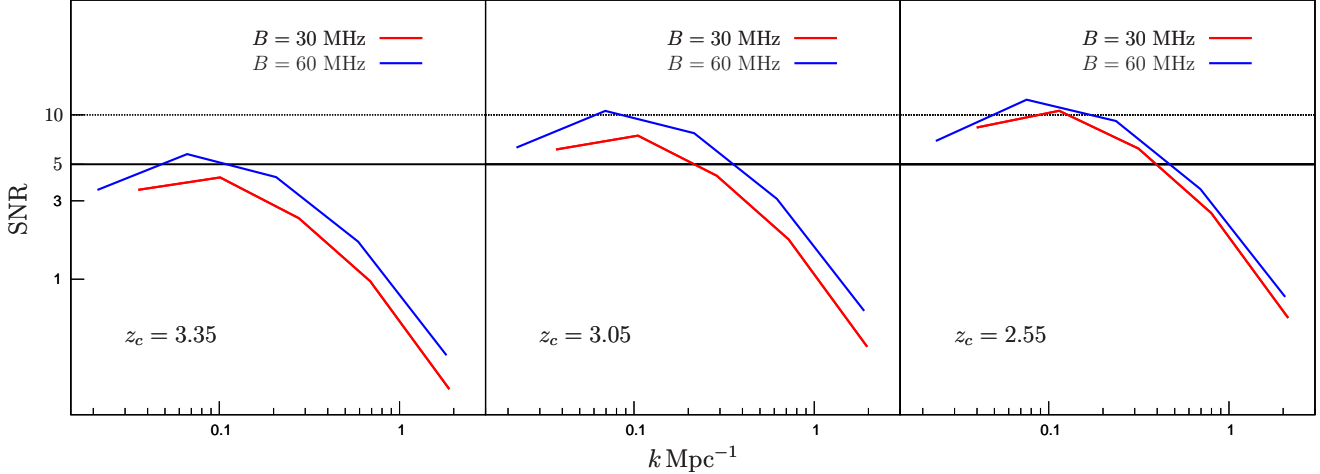


Figure 3. Shows the plot of SNR for measuring the amplitude of $\mathcal{P}_{FT}(k)$ in different k -bins with an observing time of 200 hrs each in $N_p = 25$ independent fields-of-view for the different redshifts and bandwidths considered here. The lower solid black lines and upper dash-dotted black lines correspond to $\text{SNR} = 5$ and 10 respectively.

cm auto-correlation. For $B = 60$ MHz we find $\Delta\beta_F/\beta_F \approx 0.6, 0.36$ and 0.23 at $z_c = 3.35, 3.05$ and 2.55 respectively. For $B = 30$ MHz these values go down by factors of $1.45, 1.4$ and 1.15 respectively. We see that it is possible to measure β_F with 4σ and 5σ confidence with $B = 30$ MHz and 60 MHz respectively by combining auto-correlation and cross-correlation observations at $z_c = 2.55$.

The analysis so far has assumed that the shape of the cross-correlation power spectrum $\mathcal{P}_{FT}(U, \tau_m)$ traces the dark matter power spectrum $P(k)$ (eq. 2.3). It is interesting and worthwhile to consider the possibility of constraining the shape of the cross-correlation power spectrum directly from observation. To this end we have assumed that the values of β_T and β_F are known, and we have investigated how precisely it will be possible to measure $\mathcal{P}_{FT}(k)$ using observations of the cross-correlation signal. We have binned the k range $0.018 \leq k \leq 2.73 \text{ Mpc}^{-1}$ which will be probed by OWFA PII into 5 equally spaced logarithmic k -bins and we have used the Fisher matrix technique to determine the SNR with which it would be possible to measure the amplitude of the cross-correlation power spectrum in each of these k bins. Note that the k limits change to some extent when z_c and B are varied, and we have incorporated these in our estimates.

Figure 3 shows the predicted SNR for measuring the amplitude of the cross-correlation power spectrum in different k bins. We expect the errors in the small k -bins to be dominated by cosmic variance as opposed to the larger k -bins where the errors are predominantly due to the system noise. We see that for $z_c = 3.35$ (left panel) and $B = 30$ MHz a $\text{SNR} \geq 3$ measurement is possible in the two smallest k bins, however it is not possible to achieve $\text{SNR} \sim 5$ in any of the k -bins with 200 hrs

observations in each of $N_p = 25$ independent fields considered here. If the bandwidth is increased to $B = 60$ MHz, a measurement with $\text{SNR} \geq 5$ is possible in a single k -bin which is centered at $k \approx 0.7 \text{ Mpc}^{-1}$. As mentioned earlier, we expect the SNR to increase if z_c is tuned toward the peak of the quasar distribution at $z \approx 2.25$. We find that for $z_c = 3.05$ (central panel) and $B = 30$ MHz, we can have a measurement with $\text{SNR} \geq 5$ in the two smallest k -bins ($\leq 0.1 \text{ Mpc}^{-1}$), and $\text{SNR} \sim 3$ is possible for the third smallest k -bin at $k \approx 0.3 \text{ Mpc}^{-1}$. For $B = 60$ MHz we expect $\text{SNR} \geq 5$ in the three smallest k bins with an SNR in excess of 10 in the bin centered at $k \approx 0.07 \text{ Mpc}^{-1}$. The predicted SNR values are somewhat increased at $z_c = 2.55$ (right panel) where we expect $\text{SNR} \geq 5$ in the three smallest k -bins for both $B = 30$ and 60 MHz.

6 Summary and Conclusions

We have carried out a Fisher matrix analysis to study the prospects of measuring the cross-correlation of the redshifted HI 21-cm signal and the Lyman- α forest. For the redshifted 21-cm signal we have considered an upcoming radio-interferometric array OWFA [41] whereas for the Lyman- α forest we have considered the currently available DR14 of SDSS [58]. As discussed in [34, 35], the cross-correlation signal holds advantages over the auto-correlation of the redshifted HI 21-cm signal and the Lyman- α forest in that the problem of foregrounds is less severe for the cross-correlation signal as compared to the 21-cm auto-correlation signal. Further, the cross-correlation signal is expected to be less sensitive to the discrete QSO sampling as compared to the Lyman- α forest auto-correlation signal. Both these advantages make the cross-correlation signal an important cosmological probe from the observation point-of-view.

OWFA PII is expected to operate with a bandwidth of around $B = 30$ MHz centered at 326.5 MHz which corresponds to $z_c = 3.35$. The quasar number distribution from DR14 of SDSS [58] peaks at $z = 2.25$ and falls off at higher redshifts. The number of quasars available for the cross-correlation analysis at $z_c = 3.35$ is quite low. In view of this, we have also explored the possibility of increasing the number of available quasars by tuning the OWFA observational frequency to $z_c = 3.05$ and 2.55 which are closer to the peak. In addition to this, we have also considered the possibility of increasing the bandwidth to $B = 60$ MHz.

We find that it is not possible to measure the amplitude of the cross-correlation signal with $\text{SNR} \sim 5$ using observations in a single OWFA field of view for any of the redshifts z_c and bandwidths B considered here (see Figure 1). The SNR increases very slowly at $t \geq 200$ hrs and it is not meaningful to consider deeper observation in a single FoV. We have considered $t = 200$ hrs observations each in $N_p = 25$ independent fields of view. We find (Table 1) that a 6σ detection is possible for $z_c = 3.35$ and $B = 30$ MHz. The SNR increases if z_c is reduced or B is doubled, and we $\text{SNR} \sim 17$ for $z_c = 2.25$ and $B = 60$ MHz.

We have considered the possibility of jointly measuring β_F and β_T , marginalizing over the amplitude of the cross-correlation signal. We find that the predicted errors in these two parameters are quite large and highly anti-correlated. Identifying combination of these two parameters which could be independently measured, we find that it

is at best possible to measure $\beta_F^{0.83}\beta_T^{0.55}$ at an SNR ~ 3 for $z_c = 2.55$ and $B = 60$ MHz. In order to improve the prospects further, we have considered the possibility of combining this with independent measurements of β_T from the 21-cm auto-correlation signal with an observing time of 1000 hrs each in $N_p = 5$ independent FoVs. We have SNR ≈ 4.1 and 1.67 for β_T and β_F respectively at $z_c = 3.35$ with $B = 30$ MHz. In the best case the respective SNR values are 12.8 and 5 at $z_c = 2.55$ with $B = 60$ MHz. The parameter $\beta_T = f/b_{HI}$ is sensitive to the cosmological model through the growth function f and the distribution of HI modeled using b_{HI} . Several probes of cosmological structure formation like the CMBR observations and galaxy redshift surveys put stringent bounds on the growth function f . Hence, the measurement of β_T shall immediately constrain b_{HI} , throwing valuable insights about the HI distribution in the post reionization epoch.

Finally we have considered the possibility of constraining the shape of the cross-correlation power spectrum by measuring its amplitude in different k bins. We find that for the z_c values considered here the SNR peaks at $k \approx 0.07 \text{ Mpc}^{-1}$ and 0.1 Mpc^{-1} for $B = 30$ MHz and 60 MHz respectively. For $B = 30$ MHz at $z_c = 3.35$ a SNR ≥ 5 measurement is not possible in the any of the k -bins, however a SNR ≥ 3 measurement is possible in the two smallest k bins. However a SNR ≥ 5 measurement is possible in the two and three smallest k bins at $z_c = 3.05$ and 2.55 respectively. For $B = 60$ MHz a SNR ≥ 5 measurement is possible at all three z_c values, the SNR values also increase if z_c is reduced to a value closer to the peak of the QSO distribution.

The entire analysis here is based on the assumption that 21-cm foregrounds have been modeled and removed prior to the cross-correlation, and the residual foreground contamination is restricted to the $k_{\parallel} = 0$ modes which have been discarded for the Fisher matrix. While the foreground contamination is expected to be less severe for the cross-correlation as compared to the auto-correlation, it is quite possible that the foreground contamination will extend beyond the $k_{\parallel} = 0$ modes causing a degradation of the SNR.

In conclusion we note that a 6σ detection of the cross-correlation signal will be possible with the upcoming OWFA PII using 200 hrs observation each in 25 independent pointing directions. However little else can be done beyond this using the cross-correlation signal at $z_c = 3.35$ with $B = 30$ MHz. The SNR of the cross-correlation detection can be significantly enhanced to ~ 17 if the OWFA observing redshift is tuned to $z_c = 2.55$ which is closer to the peak of the QSO distribution and the OWFA bandwidth is increased to 60 MHz. It is then possible to individually measure β_T and β_F with SNR ≥ 5 by combining the cross-correlation with 21-cm auto-correlation measurements. Further, it is also possible to measure the amplitude of the binned cross-correlation power spectrum in several bins at $k \leq 0.3 \text{ Mpc}^{-1}$.

7 Acknowledgment

AKS would like to thank Jayaram N. Chengalur for suggesting the problem. AKS would also like to acknowledge the help of Debanjan Sarkar, Siddhartha Bhattacharyya and Suman Chatterjee in writing the manuscript. AKS makes a special mention of

Tirthankar Roy Choudhury for useful discussions which helped in a better understanding of the subject.

References

- [1] K. M. Lanzetta, A. M. Wolfe and D. A. Turnshek, *The iue survey for damped lyman-alpha and lyman-limit absorption systems: Evolution of the gaseous content of the universe*, *The Astrophysical Journal* **440** (1995) 435.
- [2] T. Zafar, A. Popping and C. Péroux, *The eso uves advanced data products quasar sample-i. dataset and new n_{HI} measurements of damped absorbers*, *Astronomy & Astrophysics* **556** (2013) A140.
- [3] S. Bharadwaj, B. B. Nath and S. K. Sethi, *Using hi to probe large scale structures at $z \approx 3$* , *Journal of Astrophysics and Astronomy* **22** (2001) 21–34.
- [4] S. Bharadwaj and S. K. Sethi, *Hi fluctuations at large redshifts: I-visibility correlation*, *Journal of Astrophysics and Astronomy* **22** (2001) 293–307.
- [5] A. Loeb and J. S. B. Wyithe, *Possibility of precise measurement of the cosmological power spectrum with a dedicated survey of 21 cm emission after reionization*, *Physical Review Letters* **100** (2008) 161301.
- [6] J. S. B. Wyithe, A. Loeb and P. M. Geil, *Baryonic acoustic oscillations in 21-cm emission: a probe of dark energy out to high redshifts*, *Monthly Notices of the Royal Astronomical Society* **383** (2008) 1195–1209.
- [7] T.-C. Chang, U.-L. Pen, J. B. Peterson and P. McDonald, *Baryon acoustic oscillation intensity mapping of dark energy*, *Physical Review Letters* **100** (2008) 091303.
- [8] H.-J. Seo, S. Dodelson, J. Marriner, D. McGinnis, A. Stebbins, C. Stoughton et al., *A ground-based 21 cm baryon acoustic oscillation survey*, *The Astrophysical Journal* **721** (2010) 164.
- [9] R. Ansari, J.-E. Campagne, P. Colom, C. Magneville, J.-M. Martin, M. Moniez et al., *Baoradio: A digital pipeline for radio interferometry and 21 cm mapping of large scale structures*, *Comptes Rendus Physique* **13** (2012) 46–53.
- [10] S. Bharadwaj, S. K. Sethi and T. D. Saini, *Estimation of cosmological parameters from neutral hydrogen observations of the post-reionization epoch*, *Physical Review D* **79** (2009) 083538.
- [11] E. Visbal, A. Loeb and S. Wyithe, *Cosmological constraints from 21cm surveys after reionization*, *Journal of Cosmology and Astroparticle Physics* **2009** (2009) 030.
- [12] F. Villaescusa-Navarro, P. Bull and M. Viel, *Weighing neutrinos with cosmic neutral hydrogen*, *The Astrophysical Journal* **814** (2015) 146.
- [13] A. K. Pal and T. Guha Sarkar, *Constraining neutrino mass using the large-scale $h i$ distribution in the post-reionization epoch*, *Monthly Notices of the Royal Astronomical Society* **459** (2016) 3505–3511.
- [14] S. Saiyad Ali, S. Bharadwaj and S. K. Pandey, *Probing the bispectrum at high redshifts using 21-cm $h i$ observations*, *Monthly Notices of the Royal Astronomical Society* **366** (2006) 213–218.

- [15] T. G. Sarkar and D. K. Hazra, *Probing primordial non-gaussianity: the 3d bispectrum of ly- α forest and the redshifted 21-cm signal from the post reionization epoch*, *Journal of Cosmology and Astroparticle Physics* **2013** (2013) 002.
- [16] R. A. Croft, D. H. Weinberg, N. Katz and L. Hernquist, *Recovery of the power spectrum of mass fluctuations from observations of the ly α forest*, *The Astrophysical Journal* **495** (1998) 44.
- [17] R. A. Croft, D. H. Weinberg, M. Pettini, L. Hernquist and N. Katz, *The power spectrum of mass fluctuations measured from the ly α forest at redshift $z=2.5$* , *The Astrophysical Journal* **520** (1999) 1.
- [18] P. Macdonald et al., *The linear theory power spectrum from the lyman-alpha forest in the sloan digital sky survey*, *Astrophys. J* **635** (2005) 761.
- [19] R. Mandelbaum, P. McDonald, U. Seljak and R. Cen, *Precision cosmology from the lyman α forest: power spectrum and bispectrum*, *Monthly Notices of the Royal Astronomical Society* **344** (2003) 776–788.
- [20] R. A. Croft, D. H. Weinberg, M. Bolte, S. Burles, L. Hernquist, N. Katz et al., *Toward a precise measurement of matter clustering: Ly α forest data at redshifts 2-4*, *The Astrophysical Journal* **581** (2002) 20.
- [21] M. Viel, S. Matarrese, A. Heavens, M. Haehnelt, T.-S. Kim, V. Springel et al., *The bispectrum of the lyman α forest at z_j 2-2.4 from a large sample of uves qso absorption spectra (luqas)*, *Monthly Notices of the Royal Astronomical Society* **347** (2004) L26–L30.
- [22] H. Bi and A. F. Davidsen, *Evolution of structure in the intergalactic medium and the nature of the ly α forest*, *The Astrophysical Journal* **479** (1997) 523.
- [23] T.-S. Kim, M. Viel, M. Haehnelt, R. Carswell and S. Cristiani, *The power spectrum of the flux distribution in the lyman α forest of a large sample of uves qso absorption spectra (luqas)*, *Monthly Notices of the Royal Astronomical Society* **347** (2004) 355–366.
- [24] R. A. Croft, W. Hu and R. Dave, *Cosmological limits on the neutrino mass from the ly α forest*, *Physical Review Letters* **83** (1999) 1092.
- [25] C. Yèche, N. Palanque-Delabrouille, J. Baur and H. d. M. des Bourboux, *Constraints on neutrino masses from lyman-alpha forest power spectrum with boss and xq-100*, *Journal of Cosmology and Astroparticle Physics* **2017** (2017) 047.
- [26] P. McDonald and D. J. Eisenstein, *Dark energy and curvature from a future baryonic acoustic oscillation survey using the lyman- α forest*, *Physical Review D* **76** (2007) 063009.
- [27] S. Gallerani, T. R. Choudhury and A. Ferrara, *Constraining the reionization history with qso absorption spectra*, *Monthly Notices of the Royal Astronomical Society* **370** (2006) 1401–1421.
- [28] T. Delubac, J. Rich, S. Bailey, A. Font-Ribera, D. Kirkby, J.-M. Le Goff et al., *Baryon acoustic oscillations in the ly α forest of boss quasars*, *Astronomy & Astrophysics* **552** (2013) A96.

- [29] T. Delubac, J. E. Bautista, J. Rich, D. Kirkby, S. Bailey, A. Font-Ribera et al., *Baryon acoustic oscillations in the $ly\alpha$ forest of boss dr11 quasars*, *Astronomy & Astrophysics* **574** (2015) A59.
- [30] T. Guha Sarkar, S. Bharadwaj, T. R. Choudhury and K. K. Datta, *Cross-correlation of the hi 21-cm signal and $ly\alpha$ forest: a probe of cosmology*, *Monthly Notices of the Royal Astronomical Society* **410** (2010) 1130–1134.
- [31] A. Ghosh, S. Bharadwaj, S. S. Ali and J. N. Chengalur, *Improved foreground removal in gmrt 610 mhz observations towards redshifted 21-cm tomography*, *Monthly Notices of the Royal Astronomical Society* **418** (2011) 2584–2589.
- [32] T. Guha Sarkar, S. Bharadwaj, T. R. Choudhury and K. K. Datta, *Cross-correlation of the hi 21-cm signal and ly forest: a probe of cosmology*, *Monthly Notices of the Royal Astronomical Society* **410** (2011) 1130–1134.
- [33] T. G. Sarkar and A. A. Sen, *Cosmology and astrophysics using the post-reionization hi* , *Journal of Astrophysics and Astronomy* **37** (2016) 33.
- [34] T. G. Sarkar and S. Bharadwaj, *Predictions for bao distance estimates from the cross-correlation of the lyman- α forest and redshifted 21-cm emission*, *Journal of Cosmology and Astroparticle Physics* **2013** (2013) 023.
- [35] T. G. Sarkar and K. K. Datta, *On using large scale correlation of the ly - α forest and redshifted 21-cm signal to probe hi distribution during the post reionization era*, *Journal of Cosmology and Astroparticle Physics* **2015** (2015) 001.
- [36] I. P. Carucci, F. Villaescusa-Navarro and M. Viel, *The cross-correlation between 21 cm intensity mapping maps and the $ly\alpha$ forest in the post-reionization era*, *Journal of Cosmology and Astroparticle Physics* **2017** (2017) 001.
- [37] P. Prasad and C. Subrahmanya, *A high speed networked signal processing platform for multi-element radio telescopes*, *Experimental Astronomy* **31** (2011) 1–22.
- [38] V. R. Marthi and J. Chengalur, *Non-linear redundancy calibration*, *Monthly Notices of the Royal Astronomical Society* **437** (2013) 524–531.
- [39] G. Swarup, N. Sarma, M. Joshi, V. Kapahi, D. Bagri, S. Damle et al., *Large steerable radio telescope at ootacamund, india*, *Nature Physical Science* **230** (1971) 185.
- [40] N. Sarma, M. Joshi, D. Bagri and S. Ananthkrishnan, *Receiver system of the ooty radio telescope*, *IETE Journal of Research* **21** (1975) 110–116.
- [41] S. S. Ali and S. Bharadwaj, *Prospects for detecting the 326.5 mhz redshifted 21-cm hi signal with the ooty radio telescope (ort)*, *Journal of Astrophysics and Astronomy* **35** (2014) 157–182.
- [42] S. Bharadwaj, A. K. Sarkar and S. S. Ali, *Fisher matrix predictions for detecting the cosmological 21-cm signal with the ooty wide field array (owfa)*, *Journal of Astrophysics and Astronomy* **36** (2015) 385–398.
- [43] A. K. Sarkar, S. Bharadwaj and S. S. Ali, *Fisher matrix-based predictions for measuring the $z = 3.35$ binned 21-cm power spectrum using the ooty wide field array (owfa)*, *Journal of Astrophysics and Astronomy* **38** (2017) 14.
- [44] D. J. Eisenstein and W. Hu, *Baryonic features in the matter transfer function*, *The Astrophysical Journal* **496** (1998) 605.

- [45] P. Collaboration et al., *Planck 2013 results. xvi. cosmological parameters*, *A&A* **571** (2014) A16.
- [46] N. Palanque-Delabrouille, C. Yèche, A. Borde, J.-M. Le Goff, G. Rossi, M. Viel et al., *The one-dimensional Ly α forest power spectrum from BOSS*, *Astronomy & Astrophysics* **559** (2013) A85.
- [47] S. Bharadwaj and S. Saiyad Ali, *On using visibility correlations to probe the $H\text{I}$ distribution from the dark ages to the present epoch—i. formalism and the expected signal*, *Monthly Notices of the Royal Astronomical Society* **356** (2005) 1519–1528.
- [48] J. X. Prochaska and A. M. Wolfe, *On the (non) evolution of $H\text{I}$ gas in galaxies over cosmic time*, *The Astrophysical Journal* **696** (2009) 1543.
- [49] P. Noterdaeme, P. Petitjean, W. Carithers, I. Pâris, A. Font-Ribera, S. Bailey et al., *Column density distribution and cosmological mass density of neutral gas: Sloan digital sky survey-iii data release 9*, *Astronomy & Astrophysics* **547** (2012) L1.
- [50] J. Bagla, N. Khandai and K. K. Datta, *$H\text{I}$ as a probe of the large-scale structure in the post-reionization universe*, *Monthly Notices of the Royal Astronomical Society* **407** (2010) 567–580.
- [51] T. Guha Sarkar, S. Mitra, S. Majumdar and T. R. Choudhury, *Constraining large-scale $H\text{I}$ bias using redshifted 21-cm signal from the post-reionization epoch*, *Monthly Notices of the Royal Astronomical Society* **421** (2012) 3570–3578.
- [52] F. Villaescusa-Navarro, M. Viel, K. K. Datta and T. R. Choudhury, *Modeling the neutral hydrogen distribution in the post-reionization universe: intensity mapping*, *Journal of Cosmology and Astroparticle Physics* **2014** (2014) 050.
- [53] D. Sarkar, S. Bharadwaj and S. Anathpindika, *Modelling the post-reionization neutral hydrogen ($H\text{I}$) bias*, *Monthly Notices of the Royal Astronomical Society* **460** (2016) 4310–4319.
- [54] A. Borde, C. Yèche, N. Palanque-Delabrouille, R. Croft, A. Font, J. LeGoff et al., *Measurement of the 1d Lyman-alpha power spectrum with the DR9 BOSS quasar data*, in *American Astronomical Society Meeting Abstracts# 221*, vol. 221, 2013.
- [55] A. K. Sarkar, S. Bharadwaj and V. R. Marthi, *An analytical method to simulate the $H\text{I}$ 21-cm visibility signal for intensity mapping experiments*, *Monthly Notices of the Royal Astronomical Society* **473** (2017) 261–270.
- [56] M. F. Morales, *Power spectrum sensitivity and the design of epoch of reionization observatories*, *The Astrophysical Journal* **619** (2005) 678.
- [57] C. P. Ahn, R. Alexandroff, C. A. Prieto, F. Anders, S. F. Anderson, T. Anderton et al., *The tenth data release of the Sloan Digital Sky Survey: first spectroscopic data from the SDSS-III Apache Point Observatory Galactic Evolution Experiment*, *The Astrophysical Journal Supplement Series* **211** (2014) 17.
- [58] B. Abolfathi, D. Aguado, G. Aguilar, C. A. Prieto, A. Almeida, T. T. Ananna et al., *The fourteenth data release of the Sloan Digital Sky Survey: first spectroscopic data from the extended baryon oscillation sky survey and from the second phase of the Apache Point Observatory Galactic Evolution Experiment*, *arXiv preprint arXiv:1707.09322* (2017) .

- [59] S. Bharadwaj, A. K. Sarkar and S. S. Ali, *Fisher matrix predictions for detecting the cosmological 21-cm signal with the ooty wide field array (owfa)*, *Journal of Astrophysics and Astronomy* **36** (2015) 385–398.
- [60] S. Bajtlik, R. C. Duncan and J. P. Ostriker, *Quasar ionization of lyman-alpha clouds-the proximity effect, a probe of the ultraviolet background at high redshift*, *The Astrophysical Journal* **327** (1988) 570–583.
- [61] R. J. Weymann, R. F. Carswell and M. G. Smith, *Absorption lines in the spectra of quasistellar objects*, *Annual Review of Astronomy and Astrophysics* **19** (1981) 41–76.